High efficiency dielectrophoretic ratchet

High-efficiency dielectrophoretic ratchet

Wijnand Chr. Germs,[1] Erik M. Roeling,[1] Leo J. van IJzendoorn,[1] Barry Smalbrugge,[2] Tjibbe de Vries,[2] Erik Jan Geluk,[2] René A. J. Janssen,[1] and Martijn Kemerink[1,*]

[1]*Applied Physics, Eindhoven University of Technology, P.O. Box 513, 5600 MB Eindhoven, The Netherlands*

[2]*COBRA Research Institute, Eindhoven University of Technology, P.O. Box 513, 5600 MB Eindhoven, The Netherlands*

(Received 2 May 2012; published 2 October 2012)

Brownian ratchets enable the use of thermal motion in performing useful work. They typically employ spatial asymmetry to rectify nondirected external forces that drive the system out of equilibrium (cf. running marbles on a shaking washboard). The major application foreseen for Brownian ratchets is high-selectivity fractionation of particle or molecule distributions. Here, we investigate the functioning of an important model system, the on/off ratchet for water-suspended particles, in which interdigitated finger electrodes can be switched on and off to create a time-dependent, spatially periodic but asymmetric potential. Surprisingly, we find that mainly dielectrophoretic rather than electrophoretic forces are responsible for the ratchet effect. This has major implications for the (a)symmetry of the ratchet potential and the settings needed for optimal performance. We demonstrate that by applying a potential offset the ratchet can be optimized such that its particle displacement efficiency reaches the theoretical upper limit corresponding to the electrode geometry and particle size. Efficient fractionation based on size selectivity is therefore not only possible for charged species, but also for uncharged ones, which greatly expands the applicability range of this type of Brownian ratchet.

DOI: 10.1103/PhysRevE.86.041106 PACS number(s): 05.40.Jc, 82.45.Un, 82.70.Dd

I. INTRODUCTION

Ratchet devices are made up of repeated asymmetric units that give rise to an (asymmetric) potential landscape that resembles a washboard or a factory rooftop [1]. Particles that are subjected to both this potential and some unbiased, periodic or random time-dependent force can show a net average motion: The unbiased force is rectified by the ratchet asymmetry and drives a particle current. The "particle" can be an electron or hole [2,3], a suspended bead [4], a marble [5], a droplet [6], or even a living cell [7]. In a Brownian ratchet random thermal forces are rectified. Hence, in such devices thermal motion is not a disruptive element, but is used to perform useful work. Brownian ratchets were first introduced in a thought experiment by Smoluchowski [8]. Later, Feynman showed that ratchets can only perform work using Brownian motion when the system is taken out of thermal equilibrium [9]. A recent overview of the field is given in Ref. [1].

The first and main practical application foreseen for ratchets is the separation of particles, molecules, or even living cells [7,10–22]. It has been shown in different ratchet systems that current reversals can occur upon minute changes in one of the system parameters [1–3,21]. Achieving this for suspended particles (or molecules, cells) would allow one to have any two types of particles being transported in opposite directions, which would open the way to highly selective and small sized particle separators. The typical "*Drosophila* system" is formed by water-suspended particles that are subjected to a time-dependent ratchet-shaped potential—The example of the on/off ratchet is explained in the next section. Different sorts of "wet ratchets" have been employed, and include structured arrays for moving molecules and cells [10–12], optical ratchet traps for moving microspheres [13,14], magnetic ratchets for moving superparamagnetic beads [15–17], and electric ratchets for moving microspheres and molecules [18–22].

Of the above realizations of wet ratchets, the electric ratchets impose the least constraints on the particle to displace as they can potentially use both electrophoretic and dielectrophoretic forces and are not restricted to (superparamagnetic) magnetic particles. The electrophoretic forces result from the direct interaction between the electric field in the medium and the charge on the particles. Dielectrophoretic forces occur due to the difference in (effective) relative dielectric constant ε_r between the particle and the medium and the difference in electrostatic energy density u,

$$\Delta u = \tfrac{1}{2}\varepsilon_0(\varepsilon_{r1} - \varepsilon_{r2})|E|^2 \tag{1}$$

that follows from this. In (1) E is the local electric field. For particles in conductive media the dielectrophoretic forces are not only determined by the polarizability. Free charge can flow to the bound charge at the interface between two materials with different ε_r, changing the effective polarizability, which is known as the Maxwell-Wagner mechanism [23]. As a consequence of the finite time required for this flow, the effective polarization becomes frequency dependent. The dielectrophoretic force is then written as [24]

$$\langle \boldsymbol{F}_{\mathbf{DEP}} \rangle = \pi \varepsilon_m a^3 \mathrm{Re}\left(\frac{\tilde{\varepsilon}_p - \tilde{\varepsilon}_m}{\tilde{\varepsilon}_p + 2\tilde{\varepsilon}_m}\right)\nabla|E|^2, \tag{2}$$

with a being the particle radius, $\tilde{\varepsilon} = \varepsilon - i\sigma/\omega$ the complex permittivity of the particle (p) and medium (m) with $\varepsilon = \varepsilon_0\varepsilon_r$, ω the frequency, and σ the conductivity. The Clausius-Mossotti factor, Re( ), describes the frequency dependence and can have values between $+1$ and $-1/2$.[23] For nonconductive particles as discussed here, Eq. (2) implies that for low σ_m/ω the dielectrophoretic force is dominated by its static component [cf. Eq. (1)] and can be either positive or negative, depending on the sign of $(\varepsilon_{r,p} - \varepsilon_{r,m})$. For high σ_m/ω the force is

*m.kemerink@tue.nl

dominated by the free charges at the particle-fluid interface giving rise to negative dielectrophoresis.

In a general electrically driven wet ratchet, the dominance of electrophoretic or dielectrophoretic forces depends on subtle, and sometimes hard to control details of the system such as the surface charge of particles or the ion concentration in the medium. This issue is particularly relevant as one and the same driving signal can lead to rather different forces on the particle, depending on which force dominates; below it will be shown that a potential that is highly asymmetric for electrophoretic interactions may actually be completely symmetric for dielectrophoretic interactions. In previous works, dominance of dielectrophoresis was enforced using modulated high frequency potentials [19,21]. In contrast, when low frequency potentials were employed electrophoresis was assumed dominant [18].

Here, we use an on/off ratchet, consisting of asymmetrically spaced interdigitated electrodes on a planar substrate, to displace suspended polystyrene spheres. A major advantage of this design is that the magnitude of the potential minima and maxima, and hence the symmetry of the drive, can be independently tuned. Using both simulations and experiments we show that also at low frequency drive the potential profile experienced by the particle is dominated by dielectrophoresis. Being able to qualitatively explain the observed behavior, this knowledge can be exploited to optimize the particle displacement, bringing it to the theoretical maximum expected for this device layout and particle size: displacement data match calculations without free parameters.

II. DEVICE PRINCIPLE AND EXPERIMENTAL DETAILS

The ratchet used here, the electrical on/off ratchet, is explained in Fig. 1(a). Two sets of asymmetric interdigitated finger electrodes, AF1 and AF2, are placed on an insulating surface. When these finger electrodes are biased with different polarity, suspended charged particles present in the microchannel are trapped in the resulting asymmetric potential wells [Fig. 1(b)]. When the potential on the electrodes is switched off, the particles diffuse without a preferential direction. After a certain time the potential is switched on again. The asymmetry of the potential wells leads to an asymmetry in the retrapping. More particles have diffused over the short distance in the asymmetric repeat unit, i.e., past the electrode on the right, then over the long distance to the left. Hence, a larger fraction of particles becomes retrapped in the nearest neighbor trap on the right, then in the nearest neighbor trap on the left. The asymmetry therefore results in a net particle current. Also, when other than electrophoretic forces are present or even dominant, the device remains a ratchet as long as a spatial asymmetry in the forces is maintained.

The parameter α indicates the asymmetry and is defined as the location of the trapping position over the total length of the repeat unit, shown in Fig. 1(b); hence $\alpha = 1/2$ corresponds to a symmetric device.

The ratchets sketched in Fig. 1(a) were fabricated on Si-SiO_2 substrates. The finger electrodes have a width of 1 μm, a length of 1 mm, and a thickness of 30 nm (5 nm Ti, 25 nm Pt). The short distance between the fingers is 1 μm and the long distance is 4 μm. The electrodes are defined using

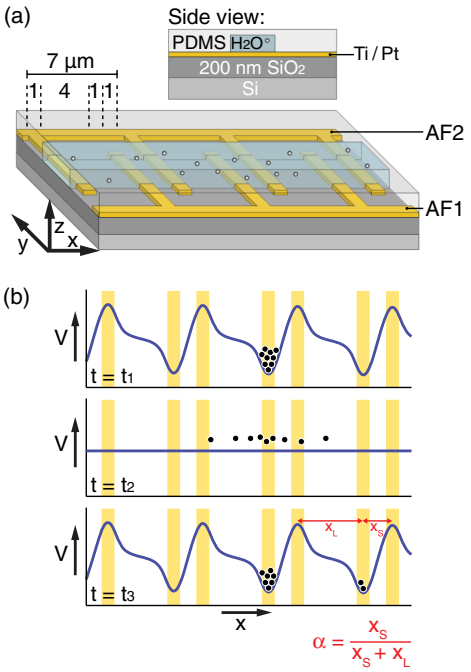

FIG. 1. (Color online) (a) Schematic overview of the ratchet device consisting of interdigitated finger electrodes on a silicon wafer with a 200 nm isolating thermal silicon dioxide layer on top. A patterned slab of PDMS is placed on top creating a 25 μm $\times$ 100 μm microchannel for the suspended particles. (b) Schematic electrostatic potential along the microchannel at three subsequent moments in time explaining the ratchet mechanism. At time t_1 all particles are in the same trap. At t_2 the electrodes are switched off allowing (undirected) diffusion. At t_3 the electrodes are switched on again; due to the asymmetry a net displacement of particles results. The cartoon assumes electrophoresis to be dominant over dielectrophoresis. The asymmetry parameter α is explained in the final ratchet trap.

conventional UV photolithography and liftoff. A patterned poly(dimethylsiloxane) (PDMS) slab with the microchannel is fabricated from a SU8 mold fabricated using photolithography.

Measurements are performed for 300 nm (Ademtech, Standard Carboxyl-Adembeads 0213) and 500 nm (Ademtech, MasterBeads Carboxylic Acid 0215) polystyrene spheres functionalized with carboxylic acid. Suspended in a 10^4 times diluted phosphate buffered saline (PBS) solution (0.015 mM) with pH 7.4, the particles are negatively charged. An optical microscope (Leica CTR6000M) with immersion objective (Leica HXC APO L63X/0.90W U-V-I) and a high speed camera were used to record the particle motion at 50 frames/s and a pixel size of 91 nm. The images were analyzed using home-written software in MATLAB from which the particle position and subsequently their movement could be determined with subpixel precision.

III. RESULTS

Typical ratchet behavior was measured for the negatively charged 300- and 500-nm polystyrene spheres. When the electrodes are turned on, electrode AF1 is biased to 375 mV and AF2 to -375 mV, defined with respect to a reference electrode outside the channel. On periods are marked by the shaded areas in Fig. 2(a). When turned off both AF1

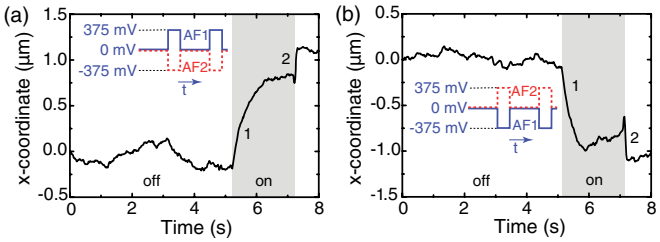

FIG. 2. (Color online) Average position during one driving cycle determined from approximately 200 particles (500 nm). Shaded areas indicate the electrodes being switched on; with (a) forward drive and (b) reverse drive, achieved by changing polarity. The insets show the driving potentials on the two electrodes.

and AF2 are set to 0 V. During the "off" period of 6 s there is little average movement and it is undirected, showing the absence of convective or other background fluid motion. The diffusive spread of the initially highly localized particle distribution does not show up in this ensemble-averaged graph of approximately 200 particles. Upon switching on the potential, the particles show an average movement (marked by a 1) which saturates when most particles reach their respective equilibrium or "trap" location. This behavior closely follows the expected on/off ratchet behavior discussed in Fig. 1(b). After 2 s, when the ratchet potential is turned off again, the particles show a short, sudden movement, marked by a 2. We tentatively attribute this unexpected motion to transient electric fields arising due to the delayed rearrangement of ions in the electrostatic double layers after the sudden change in electrode potential: Upon removal of the positive bias on AF1 the screening anions cause a repulsive force for the negatively charged beads, driving them towards AF2, i.e., in the positive x direction. Alternatively, drag forces due to redistributing ions could have a similar effect. In either case, the associated displacement is smaller than the electrode width and will therefore not break down the ratchet mechanism and convert the device to a "plain" pumping device. Actually, feature 2 turns out to be decoupled from the ratchet effect No. 1 in which we are interested and will be disregarded in the remainder of this paper: All displacements shown below refer to feature 1 only.

Figure 2(b) shows that going from forward drive to reverse drive, i.e., switching the polarity of the electrodes, results in the same behavior but in the opposite direction. This is expected from a ratchet. In the direction parallel to the electrodes no notable features could found, which is shown in Appendix A.

Figure 3(a) shows two sets of measurements in which we varied the central potential offset of the finger electrodes, while keeping the potential difference at 750 mV (see inset). The electrode potentials in the off state are still equal to 0 V. In Fig. 3(a) the average displacement is plotted versus the potential of the positive electrode. Although the figure shows that the reproducibility between sets of nominally identical experiments is still an issue, the reproducibility within each experimental run is good, which is demonstrated by the magnitudes shown in Figs. 2(a) and 2(b). As standard cleaning procedures were used, the differences between the two sets of experiments are most likely due to variations in the amount of surface charges on the SiO_2 substrates, which are notoriously

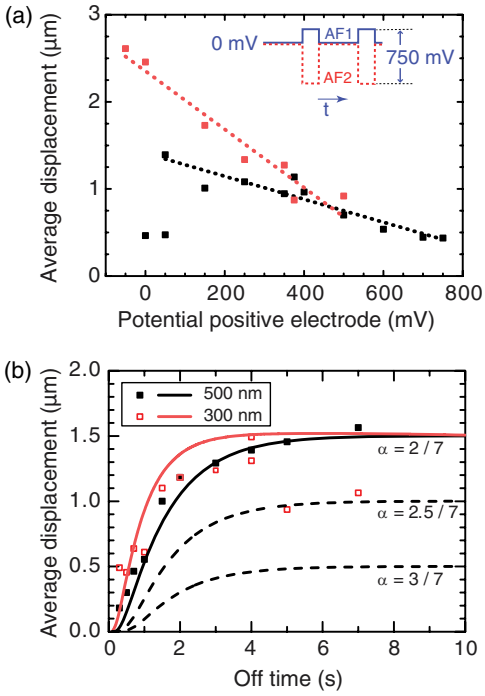

FIG. 3. (Color online) (a) Average displacement after switching the electrodes on vs the potential of the positive electrode. The potential difference between AF1 and AF2 remains 750 mV and the on (off) time is equal to 2 (6) s. The black and the red (gray) points are two sets of nominally identical measurements taken on two different days. (b) Average displacement vs the off time for two sizes of particles with electrode AF1 = 50 mV and AF2 = −700 mV. Measurements are indicated by the squares and calculations by the solid lines. Dashed lines indicate other asymmetries for 500 nm particles.

hard to control in humid or wet environments. For the present purposes this is not problematic but for real applications improved surface control is mandatory.

The experimental results in Fig. 3(a) can be considered surprising if one expects the ratchet to work due to electrophoretic forces only, as in this case the asymmetry should hardly change when only changing the offset of the electrodes. The explanation of the measurements will follow in the next section.

All the measurements up to now are done with an off time of 6 s. Figure 3(b) shows measurements of the displacement as a function of the off time using two sizes of beads. In view of the results in Fig. 3(a) the measurements are performed with an offset of −325 mV, i.e., with the positive (AF1) and negative (AF2) electrodes at 50 and −700 mV when on, respectively. The off-time dependence found is what would be expected for this type of ratchet [15,18,21,25]. For short off times, where the time to diffuse is the limiting factor of the displacement per cycle, the 300 nm particles have a larger average displacement than the 500 nm particles. This is a direct consequence of the larger diffusion constant of the smaller particles: More particles have been able to diffuse to the capture area of the nearest neighbor trap.

From the size and off-time dependence in Fig. 3(b) we conclude that applying the potential offset did not break down

the ratchet mechanism. In the next section we will discuss the origin of the offset dependence found in Fig. 3(a).

IV. DISCUSSION

A. Driving forces

Figures 2(a) and 2(b) seem to correspond to the model described in Fig. 1(b). However, the potential offset dependence of the average displacement cannot directly be explained by this model. Upon closer inspection we observed that the equilibrium trapping position in the experiments is not located above the positive electrode as expected from a dominant electrophoretic interaction. Rather, the particles accumulate in the 1 μm gap between the two electrodes [Fig. 4(a)]. An experiment with an identical device layout, but for a short interelectrode distance of 2 μm instead of 1 μm showed that the particles are in fact attracted to the edge of the positive electrode [Fig. 4(b)].

This accumulation position cannot be explained by electrophoresis. Also, electro-osmosis could, potentially, play a role in fluid motion and hence particle displacement, but cannot explain the observed static accumulation position after the particles have reached their equilibrium positions. This leaves dielectrophoresis as the explanation for the off-electrode accumulation position.

It has been shown that particles subjected to nonuniform ac-electric fields are often driven by dielectrophoretic forces [19,23]. Whether electrophoretic or dielectrophoretic forces dominate in quasistatic situations like those considered here depends on subtle details of the experimental system [23,24]. As mentioned in the Introduction, dielectrophoretic forces occur due to the different effective dielectric constants of polystyrene and water, which depend on the static dielectric constants ($\sim$2.7 and $\sim$80, respectively) and on the conductivity of the buffer solution. Depending on the frequency and the system parameters a particle will therefore be attracted to either the field maximum or the field minimum. Intuitively one might expect a high instead of a low electric field at the side of an electrode. However, in Figs. 4(c) and 4(d) we show two-dimensional finite element simulations of the static electric field in the solution along one repeat unit of the microchannel. The calculations represent the fields in the on state when the particles are trapped. These simulations were performed using COMSOL MULTIPHYSICS 3.4. When the

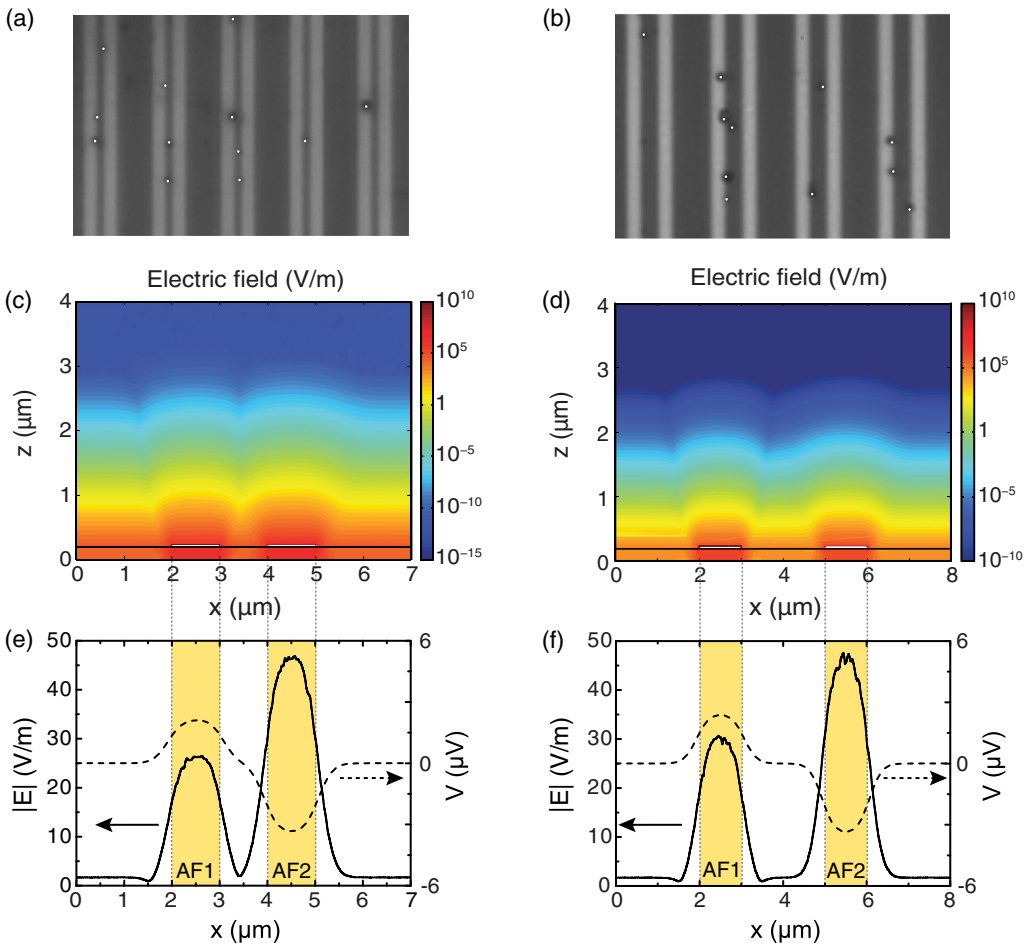

FIG. 4. (Color online) Camera image of particles in a ratchet trap with a short interelectrode distance of (a) 1 μm and (b) 2 μm. For easy recognition we added white dots to the particles. (c) and (d) Calculated total electric field magnitude for one ratchet trap unit with periodic boundary conditions. (e) and (f) Calculated electric field magnitude (solid line) at $z = 1$ μm, showing a field minimum at the position of the trapped particles. The potential (dashed line) shows only small variations in the potential at $z = 1$ μm. Potential settings are $V_{\mathrm{AF1}} = +375$ mV and $V_{\mathrm{AF2}} = -375$ mV.

particles are trapped and have reached their steady state positions, no current of any kind flows and we can assume local equilibrium holds and Boltzmann statistics can be applied. The charge carrier density is then calculated using the Boltzmann equation

$$\rho = eN_A 10^3 \sum_i z_i M_i \exp\left(-\frac{z_i e V}{k_B T}\right), \tag{3}$$

with N_A being Avogadro's number, z_i the valency of the ion species, and M_i its molarity in mol/dm^3. The surface charge on the SiO_2 was calculated to be -5.4 C/m^2 from a generalized Grahame equation

$$\sigma_{\text{surface}} = \sqrt{4\varepsilon_0 \varepsilon_r k_B T \sum_i \left[n_{0i} \exp\left(-\frac{e z_i V_0}{k_B T}\right) - 1\right]}, \tag{4}$$

with n_0 the ion concentration, k_B the Boltzmann constant, T the temperature, and V_0 the SiO_2 surface potential. More details can be found in Appendix B. Figures 4(e) and 4(f) show the electric field magnitude $|E|$ over a cross section at a height of $z = 1$ μm. The finger electrodes are biased at 375 mV (AF1, left) and -375 mV (AF2, right), i.e., with zero central offset. The field minima at the sides of the positive electrode occur due to the presence of a negative surface charge on the silicon dioxide at pH 7.4. The perpendicular component of the electric field E_z of the silicon dioxide surface is opposite to that of the positive electrode and there the superposition results in a minimum in the electric field magnitude $|E|$. Hence, dielectrophoretic interactions are expected to lead to a pileup of beads either beside the positive electrode, i.e., in the field minimum, or on top of the electrodes, i.e., in the field maxima. Electrophoresis would still pile up (negatively charged) beads on top of the positive electrode. Since the beads pile up in the field minimum we conclude that the equilibrium trapping position in the present system is dominated by negative dielectrophoresis. By disregarding the silicon dioxide surface charge the field minimum is found exactly in the middle between AF1 and AF2. This does not correspond to the trap position observed in Fig. 4(b). However, we confirmed the dominance of dielectrophoresis over electrophoresis in determining the particle trapping position by applying a fast ac (100 Hz) instead of dc potential to the electrodes, which led to a pileup of beads at the same positions as shown in Fig. 4.

Having established negative dielectrophoresis as being responsible for the equilibrium position of the beads when the electrodes are biased might suggest that the beads should move away from the bottom surface, in the direction of lower electric field [see Figs. 4(c) and 4(d)]. However, gravitational forces counteract this, leading to an equilibrium position in close vicinity of the SiO_2 surface.

Although essential to explain the trap position, the field calculation in Fig. 4 cannot explain the preferential pileup of virtually all beads on the right-hand side of the left electrode, since many particles have to pass the high field region above the left electrode to get there after switching on. This high field region is dielectrophoretically "repelling." We tentatively attribute this to transient electrophoretic forces during switching and electro-osmosis. Due to the static screening of the electric field, Fig. 4 shows negligible potential gradients between $x = 0$ and 1 μm and between $x = 6$ and 7 μm, i.e., over most of the long distance in the asymmetric repeat unit. However, in the experiments the fast motion directly after switching the potential on shows that the beads do experience a significant force in those regions shortly after switching. When the potential is switched on, the (changes in the) screening double layers need some time to form, during which the field penetrates further into the fluid, attracting the beads towards the positive electrode. Furthermore electro-osmosis can play an important role as the double layer ions can create a fluid motion that drags the particles along. Although this effect can assist particles in overcoming dielectrophoretically repelling regions, it cannot explain the lack of diffusive motion once the particles have reached their equilibrium position.

The importance of transient electric fields makes it extremely difficult to predict the particle displacement from field calculations. It becomes even more complicated due to the spread in particle height, estimated to be 0.6–6 μm (Appendix C), making it virtually impossible to even define one asymmetry α on the basis of steady state calculations. In the next section it will be shown that an "effective asymmetry" can nonetheless be determined from experimental results.

B. Symmetry considerations

We started out explaining the device using Fig. 1(b), displaying the position-dependent potential, relevant for electrophoresis. Whereas the electrophoretic force is proportional to the gradient of the potential,

$$\boldsymbol{F_E} \propto \nabla V, \tag{5}$$

the dielectrophoretic force is proportional to the gradient of the squared electric field,

$$\boldsymbol{F_D} \propto \nabla |E|^2 = \nabla |\nabla V|^2. \tag{6}$$

The dielectrophoretic analog of the ratchet potential in Fig. 1(b) would therefore show the square of the electric field magnitude $|E|^2$, i.e., $|\nabla V|^2$. This we will use to look at the asymmetry of the dielectrophoretic ratchet.

With Fig. 5 we can explain that using equal potential amplitudes on the positive and the negative electrodes (solid lines), and disregarding the SiO_2 surface charge, results in a perfectly symmetric dielectrophoretic "ratchet," from which no net particle current is to be expected. Figure 5(a) shows

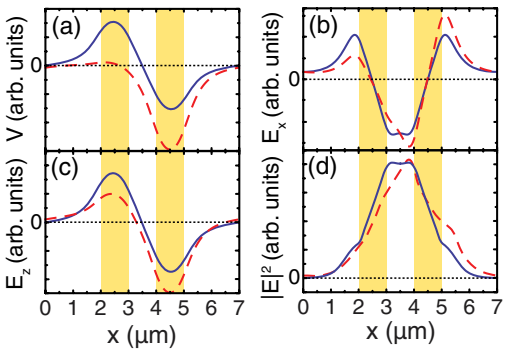

FIG. 5. (Color online) The relation between the potential profile and the symmetric $|E|^2$ profile for a ratchet without a potential offset (solid line) and the asymmetric $|E|^2$ profile with a potential offset (dashed line).

the corresponding potential; the shaded areas represent the electrode positions. Clearly, the maximum and the minimum in the potential have an equal magnitude but different sign. The field directed along the microchannel E_x is simply the derivative of this potential curve and is displayed in Fig. 5(b). Note that $E_x = dV/dx$ is inversion symmetric in $x = 3.5$ μm. Figure 5(c) shows that the field perpendicular to the SiO_2 surface, E_z, is not symmetric. However, the magnitude of E_z is symmetric. The total field squared [Fig. 5(d)] will therefore also be symmetric in $x = 3.5$ μm. Inversion asymmetry can be induced by applying an offset to the finger potentials in the on state as illustrated in the inset of Fig. 3(a). An (unintended) potential offset can also result from the SiO_2 surface charge, or from electrochemical processes at the (reference) electrode(s). To investigate the consequences of an offset to the electrode potentials the dashed line in Fig. 5 shows the potential and field if one applies an equal offset to both electrodes when turned on. Figures 5(b) and 5(c) show that the field magnitudes in the x and z directions are no longer symmetric in $x = 3.5$ μm. The latter can be understood from the three-dimensional geometry and the screening by the water: The perpendicular field E_z goes nonlinearly to zero when moving away from $z = 0$. Hence, at any given height, E_z will depend on offset; in particular, the magnitude of E_z will be different if the positive and negative electrodes have an unequal bias magnitude due to a nonzero offset. As a consequence the square of the field magnitude does have a ratchet shape now, i.e., it lacks inversion symmetry. This result tells us that asymmetric biasing of the electrodes while keeping the potential difference equal should alter the particle displacement efficiency in a dielectrophoretic ratchet. Here, we use the average displacement per on/off cycle as a measure for the displacement efficiency—a real (dimensionless) efficiency can be obtained by e.g., normalization by the ratchet period. Although the magnitudes of the electrostatic potential change, the (a)symmetry of the electrostatic potential is virtually unaffected by the asymmetric biasing.

Both data sets in Fig. 3(a) indeed show that the average displacement depends monotonically on the asymmetry in the on bias on AF1 and AF2, as anticipated for a dielectrophoretic ratchet. Unfortunately, the workable bias interval is insufficient to observe the anticipated minimum where the net potential turns symmetric and dielectrophoretic driving will be absent. Using more positive or negative biases first results in undesired fluid motion and later in hydrolysis.

Apart from the SiO_2 surface, also the Au electrode may carry a basically unknown surface charge. This makes it hard to predict whether an increase or a decrease in displacement efficiency is to be expected upon increasing the asymmetry in the on biases. Summarizing this discussion, both the observed accumulation position and the dependence of the average displacement on the potential offset can be explained by dielectrophoresis.

C. Particle displacement

The solid lines in Fig. 3(b) show the expected average displacement per cycle for the two types of polystyrene particles in this geometry, i.e., with short and long distances of 2 and 5 μm and a total repeat unit length of 7 μm. Geometrically, $\alpha = 2/7$ is expected for our geometry and this value is used in the calculations; other, potentially height-dependent values can result from the interplay between surface charges and screening and from the dynamic competition between electrophoretic and dielectrophoretic interactions, as discussed above. The calculation is very similar to those in Refs. [15,18,25], and evaluates the fraction of charges that, after diffusion from a given starting position for a time t_{off}, ends up above neighboring potential minima. This is calculated by integrating the Gaussian particle distribution at the potential well. Further details of the calculation are given in Appendix D, but it should be stressed that it contains no freely adjustable parameters. The agreement between calculation and experiment is striking, and indicates that the used bias parameters, which are at the edge of the window for stable operation, are close to optimal.

In spite of being practically impossible to determine from electric field calculations, the measurements show that the device does operate with an effective asymmetry parameter that is very close to the geometrically expected value of $\alpha = 2/7$. Even more remarkable is the fact that Fig. 3(a) suggests that decreasing the offset further, i.e., to negative values, can increase the particle displacement efficiency beyond the 1.5 μm that is expected from this electrode configuration. If this would indeed be the case, one could speculate that the most likely cause is transient effects related to ionic motion upon switching.

V. CONCLUSION

We fabricated electrical ratchets for suspended particles in water. A detailed analysis of equilibrium particle positions showed that even for low frequency driving dielectrophoretic rather than electrophoretic forces determine the particle trapping. The combination of a negative SiO_2 surface charge and a positively charged electrode creates a field minimum at the side of the positive electrode, making this the dielectrophoretical equilibrium position for the polystyrene spheres. Particle motion, in contrast, appears to be driven by dielectrophoretic, electrophoretic, and electro-osmotic interactions which we attribute to the finite time required by ions in the solution to reach equilibrium. The dominance of dielectrophoretic forces qualitatively changes the biasing scheme. However, by varying the asymmetry in the on bias applied to the interdigitated electrodes the particle displacement efficiency of the device can be tuned to its theoretically predicted maximum value. There are indications that the efficiency can go beyond this value.

ACKNOWLEDGMENTS

This work was funded by the Dutch Organisation for Scientific Research NWO (Grant No. VDI7575).

APPENDIX A: ADDITIONAL MEASUREMENTS TO CHECK RATCHET BEHAVIOR

Along the finger electrodes large average movements will be prevented by the presence of the microchannel. In fact Figs. 6(a) and 6(b) show the absence of even small traces of

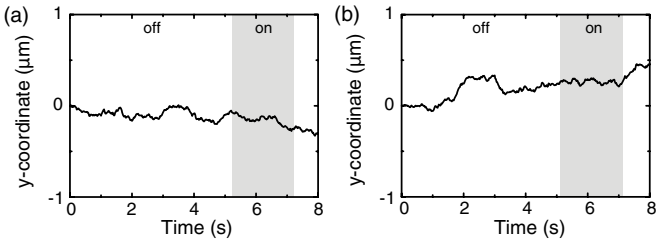

FIG. 6. Average position during one driving cycle determined from approximately 200 particles (500 nm). (a) and (b) show the movement parallel to the finger electrodes of forward and reverse drive, respectively.

switching-related lateral motion for both forward and reverse drive.

A second check for true ratchet behavior is demonstrating zero net motion by employment of a symmetric drive. The most obvious realization of such a scheme is by setting equal but antiphased amplitudes on both electrodes, which indeed yielded zero particle current (not shown) since there is no time given for diffusion. A more complex symmetric driving scheme is reached by alternating between forward and reverse driving. This leads to the average movement depicted in Fig. 2(a) followed by that of Fig. 2(b), also resulting in a negligible average movement over one complete cycle.

APPENDIX B: ELECTRIC FIELD CALCULATIONS

Calculations of the electric field and potential are performed using the COMSOL MULTIPHYSICS 3.4 package. We used the electrostatics application mode of the ac/dc module. This software performs a finite element analyses and thus solves the problem numerically.

We calculated the field for one asymmetric ratchet unit and put periodic boundary conditions to the left- and right-hand sides. Below the substrate the boundary value was set to 0 V (grounded) and at 15 μm height the boundary was set as well at 0 V (grounded), which represents the boundary value at infinity.

As explained in the main text, we calculate the fields in steady state and can therefore assume local equilibrium. The charge density was set according to the Boltzmann equation

$$\rho = eN_A 10^3 \sum_i z_i M_i \exp\left(-\frac{z_i eV}{k_B T}\right), \tag{B1}$$

with N_A being Avogadro's number, z_i the valency of the ion species, and M_i its molarity in mol/dm^3.

For the 1.5×10^{-5} M PBS solution this resulted in a charge density of

$$\rho = eN_A 10^3 \left[1.62 \times 10^{-5} \exp\left(-\frac{eV}{k_B T}\right) - 1.44 \times 10^{-5} \exp\left(\frac{eV}{k_B T}\right) - 2 \times 7.2 \times 10^{-7} \exp\left(\frac{2eV}{k_B T}\right)\right]. \tag{B2}$$

The surface charge on the SiO_2 surface can be determined using the Grahame equation, which for a monovalent solution has the form (Ref. [24])

$$\sigma_{\text{surface}} = \sqrt{8\varepsilon n_0 k_B T} \sinh\left(\frac{eV_0}{2k_B T}\right), \tag{B3}$$

with n_0 the ion concentration and V_0 the surface potential. This equation is derived by assuming that the surface charge is equal to, but opposite in sign of the total charge in the double layer.

Not assuming a monovalent solution gives a generalized Grahame equation equal to

$$\sigma_{\text{surface}} = \sqrt{4\varepsilon_0 \varepsilon_r k_B T \sum_i \left[n_{0i} \exp\left(-\frac{ez_i V_0}{k_B T}\right) - 1\right]}, \tag{B4}$$

which results in a surface charge density equal to -5.4×10^{-5} C/m^2 for SiO_2, that is used for the calculations in Fig. 4.

APPENDIX C: SPHERE-SURFACE DISTANCE

The height at which the particles float is important if the exact asymmetry of the ratchet is to be determined. Figures 4(c) and 4(d) show that the field minima change position with the distance to the device surface.

The distribution of particles as a function of distance to the SiO_2 surface can be determined from Derjaguin-Landau-Verwey-Overbeek (DLVO) theory [26,27]. First we calculate the interaction energy of the van der Waals force, the electrostatic and double layer forces, and gravitational energy. The total interaction energy is given by the sum of these energies. In Fig. 7 we show the total interaction energy as a function of the distance to the SiO_2 surface. The most likely position for particles is at the energy minimum. By using units $k_B T$ on the energy axis, one can instantly make an estimate of the typical spread of particles. A relatively short and clearly written explanation of the theory can be found in Ref. [28].

The van der Waals interaction energy for a sphere close to a surface can be written as

$$E_{\text{VDW}} = -AR/6x, \tag{C1}$$

with R being the radius of the sphere, x the distance to the surface, and A the Hamaker constant. The typical range for

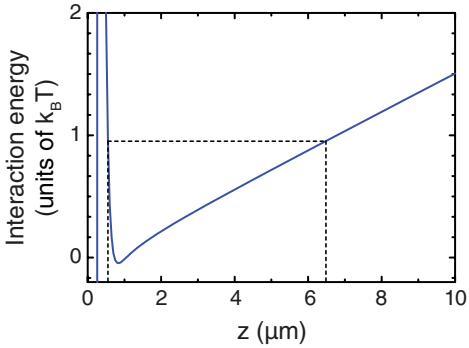

FIG. 7. (Color online) Interaction energy vs distance to a SiO_2 surface for a 500 nm polystyrene particle functionalized with carboxylic acid calculated using DLVO theory. Energy minimum is found at 800 nm from the surface. The horizontal dashed line is 1 $k_B T$ above the energy minimum.

the Hamaker constant in a liquid medium is 0.5–1.5 $\times$ 10^{-20} J (Ref. [28]); we therefore estimated it at 10^{-20} J.

The electrostatic and double layer interactions for a sphere close to a surface can be described as [28]

$$E_{\mathrm{VDW}} = RZ\ \exp(-\kappa x), \tag{C2}$$

with

$$\kappa^{-1} = \sqrt{\frac{\varepsilon_0 \varepsilon_r k_B T}{2e^2 n_0}}, \tag{C3}$$

the Debye length for a monovalent solution and n_0 the ion concentration at 0 V. The interaction coefficient Z is equal to

$$Z = 64\pi\varepsilon_0\varepsilon_r (k_B T/e)^2 \tanh\left(\frac{eV_{\mathrm{surf}}}{4k_B T}\right) \tanh\left(\frac{eV_{\mathrm{sphere}}}{4k_B T}\right), \tag{C4}$$

with V_{surf} and V_{sphere} being the SiO_2 surface potential and the sphere-surface potential, respectively.

The surface potential of the sphere, determined by the supplier, is equal to approximately -50 mV at pH 7.4. The SiO_2 surface potential we estimate at -55 ± 10 mV (Fig. 9 in Ref. [29]).

Figure 7 shows an energy minimum around 800 nm. The region within one $k_B T$ of the energy minimum ranges from 600 nm to 6.5 μm. The slope in the interaction energy above 1 μm is mainly due to the gravitation force. The uncertainty in the SiO_2 surface potential of 10 mV does not have a significant influence on these values. A 0.5 $\times$ 10^{-20} J increase (decrease) in the Hamaker constant only shifts the outer 1 $k_B T$ boundary 0.5 μm inward (outward). Comparing this width to the electric field calculations of Figs. 4(c) and 4(d), one can see that it is very difficult to computationally determine the asymmetry α, as the particles float in a region of differing asymmetry.

APPENDIX D: AVERAGE DISPLACEMENT CALCULATION

The average displacement calculation in Fig. 3(b) is performed numerically. The diffusion constant of the polystyrene spheres is calculated using the Einstein-Stokes relation

$$D = \frac{k_B T}{6\pi\eta r}, \tag{D1}$$

in which η is the viscosity and r is the particle radius. For a 500 nm sphere in water at room temperature the diffusion constant is $\sim$9.8 $\times$ 10^{-13} m^2/s and for a 300 nm sphere it is $\sim$1.6 $\times$ 10^{-12} m^2/s. Without loss of generality, the displacement upon switching the ratchet potential on is calculated for particles originating from a single trap that spread over four ratchet trap units, as displayed in Fig. 8—taking more traps into account did not significantly alter the results due to the limited diffusion distances in the off times considered. Even for an off time of 10 s, still 98.6% of all particles are taken into account. For each time t, the width $\sigma = \sqrt{(2Dt)}$ of the (Gaussian) distribution is calculated. When switching the potential on the particles are trapped in the energetically nearest trap, which is not necessarily the spatially nearest trap. With the Gaussian distribution $f(x,t_{\mathrm{off}})$ being a function of position, the average displacement in one cycle is calculated by integrating over space the product of the particle probability distribution and the resulting net displacement $X(x) = x - x_0$ upon switching the potential on again:

$$\int f(x,t_{\mathrm{off}}) X(x) dx. \tag{D2}$$

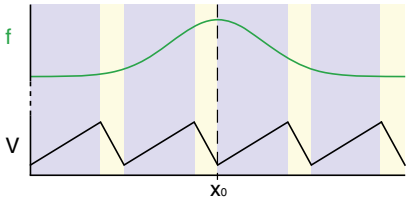

FIG. 8. (Color online) Ratchet potential V as a function of position x displayed by the lower black line. The upper green line represents a Gaussian distribution of particles at time t originating from the trap at position x_0.

[1] P. Hänggi and F. Marchesoni, Rev. Mod. Phys. **81**, 387 (2009).

[2] H. Linke, T. E. Humphrey, A. Löfgren, A. O. Sushkov, R. Newbury, R. P. Taylor, and P. Omling, Science **286**, 2314 (1999).

[3] E. M. Roeling, W. Chr. Germs, B. Smalbrugge, E. J. Geluk, T. de Vries, R. A. J. Janssen, and M. Kemerink, Nature Mater. **10**, 51 (2011).

[4] J. Rousselet, L. Salome, A. Ajdari, and J. Prost, Nature (London) **370**, 446 (1994).

[5] P. Eshuis, K. van der Weele, D. Lohse, and D. van der Meer, Phys. Rev. Lett. **104**, 248001 (2010).

[6] H. Linke, B. J. Aleman, L. D. Melling, M. J. Francis, C. C. Dow-Hygelund, V. Narayanan, R. P. Taylor, and A. Stout, Phys. Rev. Lett. **96**, 154502 (2006).

[7] G. Mahmud, C. J. Campbell, K. J. M. Bishop, Y. A. Komarova, O. Chaga, S. Soh, S. Huda, K. Kandere-Grzybowska, and B. A. Grzybowski, Nat. Phys. **5**, 606 (2009).

[8] M. von Smoluchowski, Phys. Z. **13**, 1069 (1912).

[9] R. P. Feynman, R. B. Leighton, and M. L. Sands, *The Feynman Lectures on Physics* (Addison-Wesley, Reading, 1965), Chap. 46, Vol. I.

[10] A. Oudenaarden and S. G. Boxer, Science **285**, 1046 (1999).

[11] G. Mahmud, C. J. Campbell, K. J. M. Bishop, Y. A. Komarova, O. Chaga, S. Soh, S. Huda, K. Kandere-Grzybowska, and B. A. Grzybowski, Nat. Phys. **5**, 606 (2009).

[12] S. E. Hulme, W. R. DiLuzio, S. S. Shevkoplyas, L. Turner, M. Mayer, H. C. Berg, and G. M. Whitesides, Lab Chip **8**, 1888 (2008).

[13] B. J. Lopez, N. J. Kuwada, E. M. Craig, B. R. Long, and H. Linke, Phys. Rev. Lett. **101**, 220601 (2008).
[14] L. P. Faucheux, L. S. Bourdieu, P. D. Kaplan, and A. J. Libchaber, Phys. Rev. Lett. **74**, 1504 (1995).
[15] A. Auge, A. Weddemann, F. Wittbracht, and A. Hutten, Appl. Phys. Lett. **94**, 183507 (2009).
[16] P. Tierno, P. Reimann, T. H. Johansen, and F. Sagués, Phys. Rev. Lett. **105**, 230602 (2010).
[17] L. Gao, M. A. Tahir, L. N. Virgin, and B. B. Yellen, Lab Chip **11**, 4214 (2011).
[18] J. S. Bader, R. W. Hammond, S. A. Henck, M. W. Deem, G. A. McDermott, J. M. Bustillo, J. W. Simpson, G. T. Mulhern, and J. M. Rothberg, Proc. Natl. Acad. Sci. USA **96**, 1316 (1999).
[19] E. Altintas, K. F. Böhringer, and H. Fujita, Jpn. J. Appl. Phys. **47**, 8673 (2008).
[20] C. Marquet, A. Buguin, L. Talini, and P. Silberzan, Phys. Rev. Lett. **88**, 168301 (2002).
[21] L. Gorre-Talini, S. Jeanjean, and P. Silberzan, Phys. Rev. E **56**, 2025 (1997).
[22] L. Gorre-Talini, J.P. Spatz, and P. Silberzan, Chaos **8**, 650 (1998).
[23] A. Castellanos, A. Ramos, A. Gonzalez, N. G. Green, and H. Morgan, J. Phys. D: Appl. Phys. **36**, 2584 (2003).
[24] H. Morgan and N. G. Green, in *AC Electrokinetics: Colloids and Nanoparticles* (Research Studies Press, Baldock, 2003).
[25] H. Linke, M. T. Downton, and M. J. Zuckermann, Chaos **15**, 26111 (2005).
[26] B. V. Derjaguin and L. Landau, Acta Physicochim. URSS **14**, 633 (1941).
[27] E. J. W. Verwey and J. T. G. Overbeek, in *Theory of the Stability of Lyophobic Colloids* (Elsevier, Amsterdam, 1948).
[28] D. Leckband and J. Israelachvili, Q. Rev. Biophys. **34**, 105 (2001).
[29] L. Bousse, S. Mostarshed, B. van der Shoot, N. F. De Rooij, P. Gimmel, and W. Gopel, J. Colloid Interface Sci **147**, 22 (1991).